

The impact of a wind switch on the stability of traveling fronts in a reaction-diffusion model of fire propagation

Olivia Chandrasekhar^{a,d,*}, C.K.R.T. Jones^b, Blake Barker^c, Rodman Linn^d

^a*Department of Mathematics, University of North Carolina at Chapel Hill, Chapel Hill, NC, 27599, USA*

^b*Department of Mathematics, George Mason University, Fairfax, VA, 22030, USA*

^c*Department of Mathematics, Brigham Young University, Provo, UT, 84602, USA*

^d*Earth and Environmental Sciences Division, Los Alamos National Laboratory, Los Alamos, NM, 87544, USA*

Abstract

For certain values of the wave speed parameter, evolution equations for the temperature of a region of fuel admit traveling wave solutions describing fire fronts. We consider such a system in the form of a nonlinear reaction-diffusion equation with a first-order forcing term capturing the combined effects of ambient and fire-induced wind. The fire-induced wind is introduced by way of a piecewise continuous function that “switches” in space.

We demonstrate that, in the case of a spatially dependent wind, traveling wave solutions corresponding to fire fronts exist for a continuum of wave speeds rather than for a single unique speed. Using geometric methods, we determine the range of allowable speeds, refine this range to only those fronts which will persist in nature, and develop a selection mechanism to identify the specific wind configuration corresponding to the most stable solution. For this spectrally preferred front, we find that the wind switch occurs ahead of the fireline in a manner consistent with the physics of air entrainment. Even when the wind is not coupled to the temperature and is instead imposed as an external forcing, the conditions on the existence and stability of front solutions force the wind term in to a configuration reflective of physical reality.

Keywords: fire-induced wind, traveling waves, stability, nonlinear waves

PACS: 0000, 1111

2000 MSC: 0000, 1111

1. Introduction

Understanding the spatial structure of traveling fire fronts is key to characterizing their behavior. This is true for fires at all scales, including wildfires, prescribed fires, and laboratory-scale burns. Mathematical models of fire propagation describing only the interaction between key physical quantities—such as temperature, fuel and wind—succinctly capture the dynamics and structure of the underlying physical system in a way that lends itself to rigorous mathematical analysis. Using such an approach allows us describe the complex nonlinear processes that contribute to observed behaviors and increases our ability to anticipate emergent phenomena.

In this work, we consider an example of a nonlinear reaction-diffusion equation for the evolution of the temperature of a region of homogeneous fuel. Partial differential equations of this form have been used as a minimal model for combustion in a variety of settings (including [1], [2], [3] and [4]) in part because they admit traveling wave solutions that may be used to model propagating fire fronts. We impose a spatially dependent advection term as a first-order forcing capturing the wind velocity in the vicinity of the front. Using a dynamical systems framework, we address both the existence and stability of these front solutions for qualitatively different wind configurations. We establish the concept of a spectrally preferred front by finding the minimum of the largest stable eigenvalue across all solution possibilities. Our results show that the preferred front only exists for a wind configuration consistent with the physics dictating the behavior of the wind field in the vicinity of a fire.

*Corresponding author at Los Alamos National Laboratory, Los Alamos, NM, 87544, USA. *Email address:* ochandrasekhar@lanl.gov.

A particularly important aspect of spatial and temporal analysis of fire behavior is capturing the evolution of the fireline as it propagates, where the fireline is defined as the boundary between regions of burning and unburned fuel [5]. The evolution of the fireline as a two-dimensional geometric object has been studied using, for example, level-set methods (see [6], [7]). There has also been work done to understand how local processes and environmental factors, such as fuel heterogeneity [8] and wind conditions [9], influence its shape. Generally, it is the structure of the front in the transverse direction—orthogonal to the motion of the fire—that is under consideration. See, for example, [10] for a discussion of the two-way feedback between the shape and curvature of the fireline and its dynamics in simulated grassfires.

The structure of the fire in the streamwise direction—parallel to the direction of motion—has been explored much less, although it is known that the thickness of the fireline in this direction influences the movement of the front. This thickness depends on both the speed of propagation and the residence time, or time to burn, of the fuel. In scenarios where the residence time is much larger than the ignition time—in other words, when the process of ignition occurs on a much faster time scale than the process of fuel consumption—the spatial extent of the transition zone is small. Such scenarios include most wildfires and prescribed fires (in contrast to, for example, detonations). When the timescales of the problem are separated in this way, the fireline can be conceptualized as a steep temperature profile corresponding to the initial ignition followed by a slowly declining tail as the cooling process begins to dominate. It is the initial region of transition, consisting of a steep gradient in the temperature, that we focus on in this work. See fig. 1 for a schematic diagram illustrating this region in the context of a two-dimensional fireline.

The fact that fire generates a local wind field, often referred to as the entrainment field, as the result of entrainment of cool air ahead of the fireline is well known: see [11] for an in-depth description of various wind regimes in which this occurs, [12] for a discussion of the phenomenon in coupled fire-atmosphere simulations and [13] for a mathematical treatment of the topic. The generation of this local velocity field (referred to as “pyrogenic flow” by [13] and “fire-induced wind” throughout much of this paper) is due to the buoyancy of the air heated by the combustion reaction and the principle of conservation of mass. Specifically, as air heated by combustion and burning fuel ahead of the fireline rises, cold air is pulled in to replace it.

For a straight fireline, the strongest effects from entrainment are in front of and behind the front, with the entrainment ahead of the front making a contribution to the overall velocity field in opposition to the ambient wind. In wind-driven fires, where the ambient wind is much larger than the local, fire-induced wind, a wind term that only captures the ambient wind is a reasonable estimation of reality. As a first-order approximation, this wind field may be thought of as constant in space. However, in regimes where the environmental and fire-induced wind are on the same order of magnitude, a wind term that changes in value in space is necessary to capture the entrainment field and its interactions with the ambient wind.

The implication of this three-dimensional entrainment phenomenology in a one-dimensional problem is that, in the vicinity of the traveling front, the local velocity field in the streamwise direction changes in magnitude and, potentially, reverses direction. We refer to this behavior as “switching” in the wind field. In this paper, we consider a generalized spatially dependent wind term that captures this switching behavior and explore how the constraints on existence and stability of solutions to a minimal model of fire propagation dictate the wind configuration that corresponds to the mathematically preferred solution.

Specifically, we consider a one-dimensional, nonlinear reaction-diffusion equation for the temperature of a region of burning fuel. The existence and stability of traveling wave solutions in the constant wind case to equations of this form is well understood: see [14] for the general theory. For a spatially dependent wind term, these issues are less well understood. Through a combination of geometric arguments and numerical calculations, we demonstrate the existence of traveling front solutions for a range of wave speed values dependent on the wind regime parameters. We further demonstrate that the stability properties of these solutions depend on the qualitative nature of the wind field.

These results give us tools to better understand the properties of the solution that will persist in nature in a system with a spatially dependent wind. We define the spectrally preferred front as the solution for which the corresponding largest eigenvalue is minimized and identify the unique speed at which this preferred front travels as well as the spatial location of the fire front relative to the wind switch. These findings allow us to identify, for a given wind configuration, the expected distance between and relative location of the fireline and the wind switch. We find that, for the spectrally preferred solution, the wind switch occurs ahead of the fireline. This reflects the physical motivation described above: propagating fires will entrain cool air ahead of the fireline. It is noteworthy that, despite not modeling the wind or coupling it to the temperature, this minimal, temperature-based model of fire propagation is able to describe a

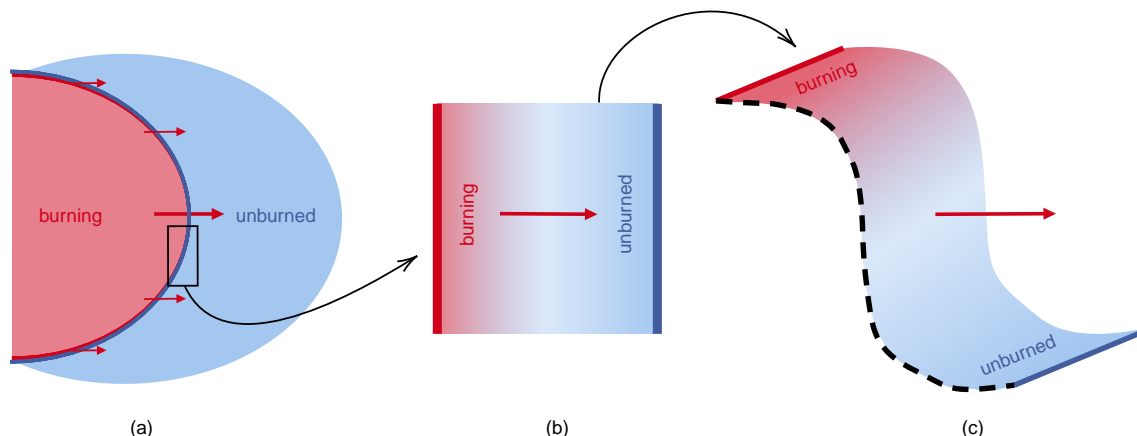


Figure 1: The fireline depicted as the boundary between regions of burning and unburned fuel in (a), then zoomed in to illustrate the transition zone between burning and unburned fuel in (b), then viewed again as a two-dimensional object in (c). The profile solutions we consider in this work correspond to the dotted black line in figure (c), asymptotically connecting regions of maximum and ambient temperature (corresponding to regions of burning and unburned fuel). The direction of motion of the fireline and the traveling wave is indicated by the red arrow(s) across all three figures.

physically relevant fire-induced wind.

2. The model

We begin with the following model, modified from [1], for the evolution of the temperature $u(x, t)$ of the fire layer, consisting of a fixed, one-dimensional region of homogeneous fuel and the layer of air immediately above it.

$$\frac{\partial u}{\partial t} = \frac{\partial^2 u}{\partial x^2} - w \frac{\partial u}{\partial x} + v^* r(u) - lu \quad (1)$$

This model has elements of diffusion due to radiative heat transfer, advection due to the local wind velocity, a nonlinear reaction term representing combustion, and loss of heat to the atmosphere due to convective heat transfer. We assume this latter effect dominates radiative heat transfer, resulting in the linear form of the loss term $-lu$, where l dictates the rate of heat loss to the surrounding environment. The parameter $v^* \in [0, 1]$ represents the fraction of the potential fuel load available at the beginning of the reaction and the advection coefficient w is the wind velocity term.

The piecewise continuous, Arrhenius-type source term ties the combustion reaction to the temperature of the fire layer and is defined as

$$r(u) = \begin{cases} e^{-1/u} & u > 0 \\ 0 & u \leq 0 \end{cases} \quad (2)$$

3. Traveling wave solutions

Systems of the form (1) are known to admit traveling front solutions connecting stationary states of the underlying system. In this model, these front solutions connect regions of high temperature to regions of ambient, or zero, temperature. As such, they may be used as a proxy to study the propagating fire fronts seen in all manner of experimental, natural and simulated fires.

To center ourselves in the frame of reference of the front solutions, we convert to traveling coordinates through the change of variable $z = x - ct$ where c is the speed of the traveling wave, resulting in

$$\frac{\partial u}{\partial t} = \frac{\partial^2 u}{\partial z^2} + (c - w(z)) \frac{\partial u}{\partial z} + v^* r(u) - lu \quad (3)$$

Note that we have introduced spatial dependence to the wind term in the frame of the fire front. The equation governing front solutions, which have spatial structure but do not change in time, is given by

$$0 = \frac{\partial^2 u}{\partial z^2} + (c - w(z)) \frac{\partial u}{\partial z} + v^* r(u) - lu \quad (4)$$

Solutions to (4) are traveling waves connecting regions of ambient temperature to regions of maximum temperature, where the maximum temperature is determined as a function of the initial fuel load v^* . As a first order system, (4) becomes

$$\begin{aligned} u' &= s \\ s' &= -(c - w(z))s - v^* r(u) + lu \end{aligned} \quad (5)$$

Fixed points of this system occur at zeros of the reaction term

$$f(u, v^*) = v^* r(u) - lu \quad (6)$$

which has a quasi-cubic structure reflective of the underlying bistability of the problem. For values of v^* above some threshold, $f(u, v^*)$ has three roots: u_0 , the ambient temperature (zero for the nondimensionalized system), u_1 , the ‘‘auto-ignition’’ temperature, representing the temperature above which the reaction becomes self-sustaining, and u_2 , the maximum temperature the system can reach given the initial fuel load v^* .

For notational clarity, in what follows we will omit the parameter v^* in the statement of (6) and simply write $f(u)$ to denote the reaction term.

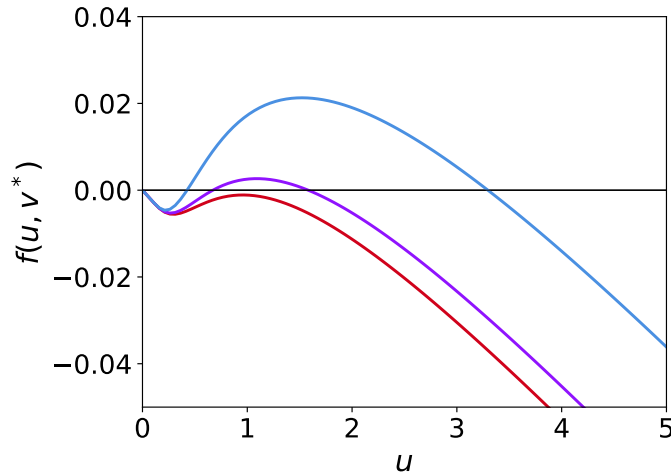


Figure 2: The reaction term $f(u, v^*)$ for three values of $v^* \in [0.07, 0.08, 0.12]$. Note that $v^* = 0.07$, indicated in red, is below the threshold for bistability. For all values of v^* above the threshold value ($v^* \approx 0.073$), $f(u, v^*)$ has three roots.

4. Constant wind

In the case when the wind term is homogeneous in space, the traveling wave solutions described in §3 are heteroclinic connections between the fixed points found as zeros of (6). In the context of the ODE system (5) with such a wind term, $(u_0, 0)$ and $(u_2, 0)$ are saddles. These points define boundary conditions for the traveling wave in the (u, s) system: as we take our traveling coordinate z to negative infinity, the solution trajectory asymptotically approaches the point $(0, 0)$. As we take our traveling coordinate z to positive infinity, it approaches $(u_2, 0)$.

Classical theory tells us that solutions \hat{u} to the corresponding second-order system (4) with a constant wind term exist only for a unique wave speed $c = \hat{c}$ (see [15]). We outline two approaches for finding these solutions.

4.1. Solutions in phase space

The first method exploits the geometric structure described above. We reframe the first order system (5) as two initial value problems, one initiated near $(u_0, s_0) = (0, 0)$ and one near $(u_0, s_0) = (u_2, 0)$. The wave speed c is a free parameter, and one can numerically integrate forwards from $(0, 0)$ and backwards from $(u_2, 0)$ to obtain solution trajectories for each initial value problem and choice of c . The c value for which these solution trajectories coincide in a single, heteroclinic orbit is \hat{c} , the unique wave speed for which a profile solution exists. These solutions exist in phase space. However, reframing them in $(z, u(z))$ space—with the proper parameterization—allows us to reconstruct the profile solution.

4.2. Solutions to the boundary value problem

The second option bypasses the phase space point of view entirely and instead considers the second-order system (4) as a boundary value problem with boundary conditions given by

$$\begin{aligned} \lim_{z \rightarrow -\infty} \hat{u}(z) &= 0 \\ \lim_{z \rightarrow \infty} \hat{u}(z) &= u_2 \end{aligned} \tag{7}$$

The wave speed c is a free parameter that is solved for alongside u .

The boundary value approach is efficient and allows us to easily specify the desired error tolerance when solving for \hat{c} . Either method allows us to find profile solutions and wave speeds that vary as a function of the initial fuel load parameter v^* . A key point is that, for all values of $v^* \in [0, 1]$, $\hat{c} < 0$. This aligns with our physical understanding that the traveling front moves from regions of maximum temperature (representing burning fuel) to regions of ambient temperature (representing unburned fuel) as the fire progresses. The sign of \hat{c} will also be an important point in our investigation of the system with a spatially dependent wind.

4.3. Stability

We linearize the second order problem (3) about solutions to (4), denoted \hat{u} . The resulting eigenvalue problem in linearized coordinates p is

$$\lambda p = \mathcal{L}p := p_{zz} + (c - w)p_z + f'(\hat{u})p \tag{8}$$

where

$$f'(u(z)) = \begin{cases} \frac{v^*}{u^2} \exp\left(-\frac{1}{u}\right) - l & u(z) > 0 \\ -l & u(z) = 0 \end{cases} \tag{9}$$

It is well known (see [16]) that the boundary of the essential spectrum of the operator \mathcal{L} associated with (8) is given by the spectrum of the operator $\mathcal{L}^{\pm\infty}$, where the latter is determined by evaluating \mathcal{L} at the profile solution \hat{u} and taking the limit as $z \rightarrow \pm\infty$. A straightforward algebraic argument demonstrates that the essential spectrum lies in the left half-plane. For details as to how this calculation works in a similar system, see [4]. There is also an eigenvalue at the origin reflective of the translational invariance of the traveling wave (see [17]): the monotonicity of the profile and an application of Sturm-Liouville theory tells us that the translational eigenvalue is the largest eigenvalue for any given solution (for details, see [18]). This in turn implies that the wave is spectrally stable.

The conclusion is that, in the spatially homogeneous wind case, profile solutions exist to (3) that move with a unique wave speed. These solutions are spectrally stable for all values of the wind speed and translates of the front are also solutions. We will see that, in the spatially dependent wind case, these results do not hold: solutions exist for a continuum of wave speeds and translational invariance is broken.

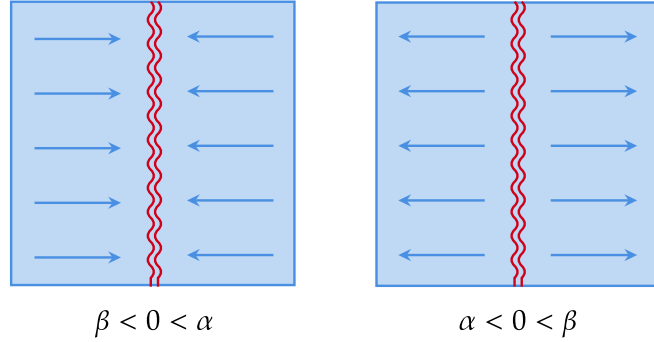


Figure 3: Two possibilities for the spatially dependent wind configuration. The first illustrates a convergent wind field and the second a divergent wind field. The fireline is indicated in red.

5. Constructing the spatially dependent wind

To introduce the switching phenomenon described in §1, we use a discontinuous step function whose magnitude is controlled by the parameters α and β :

$$w(z) = \begin{cases} \alpha & z < 0 \\ 0 & z = 0 \\ \beta & z > 0 \end{cases} \quad (10)$$

This leaves us with two potential situations: either $\alpha > \beta$ or $\alpha < \beta$. As a special case of the first option, we might consider the situation in which $\beta < 0 < \alpha$, resulting in a wind field that converges at the fireline. Alternatively, as a special case of the second option, we consider $\alpha < 0 < \beta$, resulting in a divergent wind field. The first case describes the fire-induced wind introduced in §1. The second case is physically unlikely, but presents a relevant mathematical foil that will help us better understand the physical implications of our results.

Recall that in the case of constant wind, traveling wave solutions exist for a unique \hat{c} . In the spatially dependent wind case, the situation is more complicated: solutions exist for a range of c values, each corresponding to a different profile shape. We will use the structure outlined in §4 as a guide for our analysis of the spatially dependent wind case.

6. Solutions in phase space with a spatially dependent wind

With the nonconstant wind term (10) the ODE governing the front solutions (5) is now non-autonomous. As a first order autonomous system, this becomes

$$\begin{cases} u' = s \\ s' = -(c - w(z))s - v^*r(u) + lu \\ z' = 1 \end{cases} \quad (11)$$

The system (11) has traveling wave solutions $\hat{u}(z)$ that exist for some bounded continuum of wave speeds c . There exists a set of orbits connecting the point $(u, s) = (0, 0)$ as $z \rightarrow -\infty$ and the point $(u, s) = (u_2, 0)$ as $z \rightarrow +\infty$. We can think of the dynamics projected onto the plane $z' = 1$ and therefore reduced to a 2d phase space in which both of these points are equilibria. The unstable manifold of the first fixed point is a 2d structure that intersects with the Poincaré section at $z = 0$ in a 1d curve, as is the stable manifold of the second fixed point. The point of intersection of these 1d curves on the plane $z = 0$ can then be traced back to the fixed points at $\pm\infty$ to form the heteroclinic connection, as illustrated in figure 4.

This view gives us two different systems for $z < 0$ and $z > 0$.

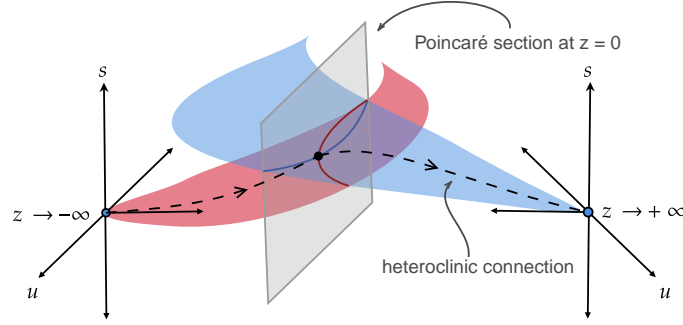


Figure 4: The 3d phase space described in §5. The blue plane is the stable manifold of the fixed point $(u_2, 0)$ for the system at $+\infty$ and the red plane is the unstable manifold of the fixed point $(0, 0)$ for the system at $-\infty$. The solid blue and red curves indicate the intersections of these manifolds with the plane $z = 0$. The point of intersection of the solid curves can be traced back across the unstable manifold and forward across the stable manifold to find the heteroclinic connection between $(0, 0)$ and $(u_2, 0)$.

For $z < 0$:

$$\begin{aligned} u'_- &= s_- \\ s'_- &= -c_1^* s_- - f(u_-) \end{aligned} \quad (12)$$

where $c_1^* = c - \alpha$. For $z > 0$:

$$\begin{aligned} u'_+ &= s_+ \\ s'_+ &= -c_2^* s_+ - f(u_+) \end{aligned} \quad (13)$$

where $c_2^* = c - \beta$. Values of c for which solution trajectories to the systems (12) and (13) intersect are values of c for which a solution exists to the full system (5) with the wind switch.

To find these values we consider solution trajectories for (12) originating at the fixed point $(0, 0)$ and tangent to the unstable subspace of that fixed point as well as trajectories for (13) originating at the fixed point $(u_2, 0)$ tangent to the stable subspace for that system. These trajectories are invariant manifolds for their respective system parameterized by the wave speed c , which is common to both systems.

The point of intersection of the manifolds corresponds to the location of the wind switch and the point on the profile where the derivative $u' = s$ is maximized corresponds to the location of the fireline. We may pick our parameterization based on either of these points: a natural choice, since we define the wind switch as occurring at $z = 0$ in (10), is to fix the point of intersection of the manifolds at $z = 0$.

6.1. Finding the invariant manifolds and their intersections

The fixed points of (12) and (13) are the same as the fixed points of (5) in the constant wind case and so are given by the zeros of (6). Again, they are saddles. Denoting a fixed point (u, s) of either system as $(u^*, 0)$, the matrix associated with the linearization of the system about the fixed point is

$$M_{\pm} = \begin{bmatrix} 0 & 1 \\ -f'(u^*) & -c^* \end{bmatrix} \quad (14)$$

where $c^* = c_1^*$ or c_2^* as appropriate and f' is defined as in (9). For the fixed point $(u_2, 0)$ at positive infinity, the stable eigenvalue of the linearization is

$$\lambda_s = \frac{-c_2^* - \sqrt{c_2^{*2} - 4(f'(u_2))}}{2} \quad (15)$$

and the corresponding eigenvector is

$$\pm \vec{v}_s = \pm \begin{pmatrix} 1 \\ \lambda_s \end{pmatrix} \quad (16)$$

Similarly, for the fixed point $(0, 0)$ at negative infinity, the unstable eigenvalue of the linearization is

$$\lambda_s = \frac{-c_1^* - \sqrt{c_1^{*2} + 4l}}{2} \quad (17)$$

and the corresponding eigenvector is

$$\pm \vec{v}_{us} = \pm \begin{pmatrix} 1 \\ \lambda_{us} \end{pmatrix} \quad (18)$$

We perturb the fixed point at $-\infty$ in the unstable direction to determine an initial condition. We then integrate forward from this initial condition to find the unstable manifold, treating our PDE as an initial value problem. We take a similar approach for the stable manifold originating from the fixed point at $+\infty$. The range of c values for which intersections exist depends on the relative values of the wind speed parameters α and β . These results are summarized in Proposition 1.

Proposition 1. *If $\alpha > \beta$, the unstable manifold of the fixed point $(0, 0)$ of (12) intersects the stable manifold of the fixed point $(u_2, 0)$ of (13) when $c_1^* < \hat{c}$ and $c_2^* > \hat{c}$, where \hat{c} is the unique wave speed for which solutions exist when $\alpha = \beta = 0$ (or equivalently, the wind is constant across the spatial domain). If $\alpha < \beta$, this intersection occurs for $c_1^* > \hat{c}$ and $c_2^* < \hat{c}$. This corresponds to $\hat{c} + \alpha < c < \hat{c} + \beta$ when $\alpha > \beta$ and $\hat{c} + \beta < c < \hat{c} + \alpha$ when $\alpha < \beta$.*

Proof. We consider $\mathcal{W}_0^u(c)$, the unstable manifold originating at $(0, 0)$ representing a solution trajectory of (12) with initial condition $(0, 0)$ and speed c . $\mathcal{W}_0^u(c)$ is parameterized in forward “time,” meaning that the independent variable z goes from $-\infty$ to $+\infty$ along the course of the trajectory.

$\mathcal{W}_{u_2}^s(c)$ is the stable manifold originating from $(u_2, 0)$ representing a solution trajectory of (13) with initial condition $(u_2, 0)$ and speed c . $\mathcal{W}_{u_2}^s(c)$ is parameterized in backward “time,” so the independent variable z goes from $+\infty$ to $-\infty$ along the course of the trajectory. Note that when $c = \hat{c}$ these manifolds coincide, meaning $\mathcal{W}_{u_2}^s(\hat{c}) = \mathcal{W}_0^u(\hat{c})$.

$\mathcal{W}_{u_2}^s(c)$ and $\mathcal{W}_0^u(c)$ are parameterized by the same wave speed c , which may or may not be a value of c for which there is a solution for the entire system with the wind switch. For values of c for which $\mathcal{W}_{u_2}^s(c)$ and $\mathcal{W}_0^u(c)$ intersect, there is such a solution.

We also consider the energy of the system, defined by the Hamiltonian associated with (5) when $c^* = 0$:

$$H(u, s) = \frac{1}{2}s^2 + \int_0^u f(r)dr \quad (19)$$

The derivative of (19) along trajectories is

$$\frac{d}{dz}H(u(z), s(z)) = -c^*s^2 \quad (20)$$

If $c^* = 0$, $\frac{dH}{dz}$ is also zero along trajectories, meaning H is constant along trajectories, so level sets of (19) are solution trajectories of (5).

The derivative of the Hamiltonian, (20), gives us information about the rate of change of energy along trajectories when $c^* \neq 0$. In particular, recall that $\hat{c} < 0$ for $v^* \in [0, 1]$. In the case of constant wind, this means that $c^* = \hat{c} < 0 \implies \frac{dH}{dz} > 0$, meaning energy is increasing along trajectories that are parameterized in forward z and decreasing along trajectories parameterized in backward z .

6.2. Case 1: $\alpha > \beta$

Consider $c_1^* = c - \alpha$. Assuming non-constant wind, either (a) $c_1^* > \hat{c}$ or (b) $c_1^* < \hat{c}$. If option (a) holds, $\frac{dH}{dz}(c_1^*) < \frac{dH}{dz}(\hat{c})$, meaning that energy increases less along the trajectories defined by $\mathcal{W}_0^u(c_1^*)$ than those defined by $\mathcal{W}_0^u(\hat{c})$. This, combined with the fact that the second component of the eigenvector from $(0, 0)$ in the unstable direction is given by the unstable eigenvalue (17) so that $c_1^* > \hat{c} \implies \lambda_{us}(c_1^*) < \lambda_{us}(\hat{c})$, means that trajectories $\mathcal{W}_0^u(c_1^*)$ will always lie below trajectories $\mathcal{W}_0^u(\hat{c})$ in phase space for case (a). If $\mathcal{W}_{u_2}^s(c_2^*)$ is to intersect $\mathcal{W}_0^u(c_1^*)$ it must also lie below $\mathcal{W}_0^u(\hat{c}) = \mathcal{W}_{u_2}^s(\hat{c})$. Because $\mathcal{W}_{u_2}^s$ is parameterized in backwards z , this requires $\frac{dH}{dz}(c_2^*) > \frac{dH}{dz}(\hat{c})$ in forward z .

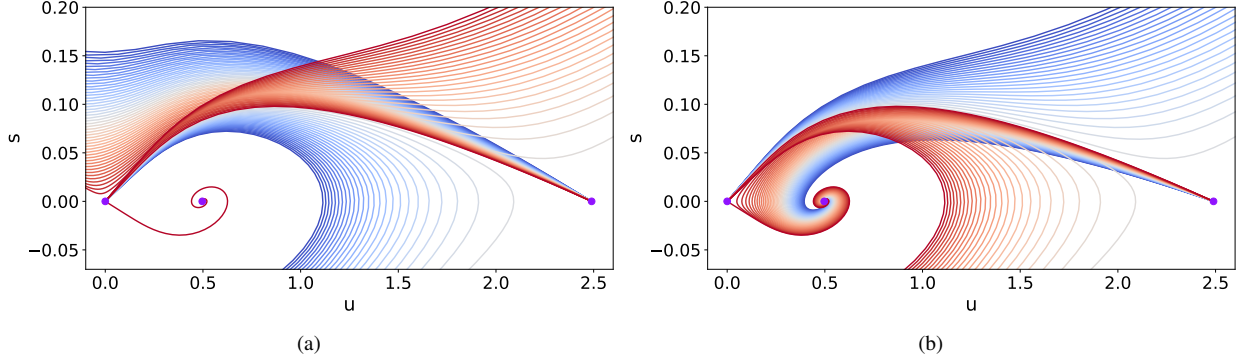


Figure 5: Invariant manifolds color-coded by wave speed value c . (a) depicts type 1 intersections for $c \in [-0.04547148, -0.12547148]$, while (b) depicts type 2 intersections for $c \in [-0.12547148, -0.04547148]$. The fixed points $(0, 0)$, $(u_1, 0)$ and $(u_2, 0)$ are indicated in purple. Note the different qualitative nature of the intersections in (a) vs. those in (b).

This implies that $c_2^* < \hat{c} \implies c - \beta < \hat{c} \implies c < \hat{c} + \beta$, and the condition on the stable manifold gives $c > \hat{c} + \alpha$. But this implies $\alpha < \beta$, contradicting our initial assumption.

So it must be that option (b) holds, meaning that $\frac{dH}{dz}(c_1^*) > \frac{dH}{dz}(\hat{c})$, meaning that energy increases more along the trajectories defined by $\mathcal{W}_0^u(c_1^*)$ than those defined by $\mathcal{W}_0^u(\hat{c})$. In this case, $\lambda_{us}(c_1^*) > \lambda_{us}(\hat{c})$, which means that trajectories $\mathcal{W}_0^u(c_1^*)$ will always lie above trajectories $\mathcal{W}_0^u(\hat{c})$ in phase space. This implies that $c_2^* > \hat{c}$ and therefore $\hat{c} + \beta < c < \hat{c} + \alpha$, which is consistent with our initial assumption that $\alpha > \beta$.

To demonstrate that $\mathcal{W}_0^u(\hat{c})$ and $\mathcal{W}_{u_2}^s(\hat{c})$ do in fact intersect for $c_1^* < \hat{c} < c_2^*$, consider the lines $u = 0$ and $u = u_2$. We know that \mathcal{W}^u originates at the point $(0, 0)$ on the line $u = 0$ and, because it is bounded, must intersect the line $u = u_2$. An analogous argument holds for \mathcal{W}^s and the line $u = 0$.

To see that the manifolds are bounded, we make the change of variables $s(z) = \exp(-c^*z)b(z)$. Then, the ODE for s' in (5) becomes $b' = -f(u)$. Integrating, we find

$$b(z) = - \int_{-\infty}^{\infty} f(u(z)) dz$$

The right hand side is bounded for $u \in [0, u_2]$ (see figure 1), so we may conclude that $s(z)$ is also bounded in that range.

Interpreting \mathcal{W}^s and \mathcal{W}^u as functions $\mathcal{W} : u \rightarrow s$, we further define $\mathbf{d}(u) = s_1(u) - s_2(u)$, where $s_2 = \mathcal{W}^s(u)$ and $s_1 = \mathcal{W}^u(u)$. The energy argument above tells us that s_1 and s_2 lie above the u axis. So, we have:

$$\begin{aligned} \mathbf{d}(u = 0) &= 0 - s_2(0) < 0 \\ \mathbf{d}(u = u_2) &= s_1(u_2) - 0 > 0 \end{aligned} \tag{21}$$

Both \mathcal{W}^u and \mathcal{W}^s are continuous functions of z because they are solution trajectories parameterized in z . Further, the fact that u is a monotone bounded function of z follows from the fact that $s > 0 \implies u' = s > 0$ and s is bounded, as demonstrated in part (1). This, together with the fact that $u(z)$ satisfies the intermediate value property for $z \in (-\infty, \infty)$, gives us that u is a continuous function of z . Therefore its inverse, $z(u)$, is also continuous. Because the composition of continuous functions is continuous, we conclude that both \mathcal{W}^u and \mathcal{W}^s are continuous functions of u . Finally, because \mathbf{d} is a continuous function of u and switches signs in the interval $[0, u_2]$, there must be a point $u^* \in [0, u_2]$ such that $\mathbf{d}(\mathcal{W}_0^u(c_1^*), \mathcal{W}_{u_2}^s(c_2^*), u^*) = 0$, meaning that \mathcal{W}_0^u and $\mathcal{W}_{u_2}^s$ intersect at this point.

6.3. Case 2: $\alpha < \beta$

By the same logic as case 1, we must have $c_2^* < \hat{c}$ and $c_1^* > \hat{c}$ in order for \mathcal{W}_0^u and $\mathcal{W}_{u_2}^s$ to intersect, giving us $\hat{c} + \alpha < c < \hat{c} + \beta$. In this case, the sign of $\frac{dH}{dz}$ and the magnitude of the eigenvector in the stable direction tells us that $\mathcal{W}_0^u(c_1^*)$ and $\mathcal{W}_{u_2}^s(c_2^*)$ must both lie below $\mathcal{W}_{u_2}^s(\hat{c}) = \mathcal{W}_0^u(\hat{c})$.

The fixed point $(u_1, 0)$ is either an unstable node or an unstable spiral for the systems from both $-\infty$ and $+\infty$. This implies that $(u, s) = (u_1, 0)$ is the α limit set of the system from positive infinity, meaning that $\mathcal{W}_{u_2}^s$ must approach the point $(u_1, 0)$ as $z \rightarrow -\infty$.

If $(u_1, 0)$ is a node for this system, this guarantees that the trajectory from $+\infty$ asymptotically approaches the point $(u_1, 0)$. On the other hand, because $(u_1, 0)$ is an unstable fixed point for the system from $-\infty$, which is parameterized in forward time, the ω limit set does not exist. Therefore, the trajectory from $-\infty$ diverges as $z \rightarrow +\infty$.

To see that solution trajectories for the systems at both $\pm\infty$ must cross the u axis in specific regions, consider the vector field along that axis:

$$\begin{aligned} u' &= 0 \\ s' &= -f(u) \end{aligned}$$

where the graph of $-f(u)$ is positive for $0 < u < u_1$ and negative for $u_1 < u < u_2$.

It follows that if \mathcal{W}_0^u is to intersect the u axis, it must do so in the region $u > u_1$ due to the direction of the vector field along the axis. The opposite is true for $\mathcal{W}_{u_2}^s$, as it is parameterized in backwards z : if it intersects the u axis, it must do so in the region $u < u_1$. Because the solution trajectories to both systems are bounded and lie below the trajectory associated with \hat{c} , which intersects the u axis, they must both intersect it as well: the above bounds on where they may do so means that they must also intersect each other. \square

6.4. Stability properties of different intersection types

We now have a natural means of classifying intersection types: either $\alpha < \beta$, resulting in “type 1” intersections, or $\beta < \alpha$, resulting in “type 2” intersections. Numerical investigation (see figure 4) reveals that these two types of intersections are qualitatively different, and this qualitative difference translates to a difference in the stability properties of the intersections. These properties are summarized in Proposition 2.

Proposition 2. *Intersections of type 1 correspond to stable fronts while intersections of type 2 correspond to unstable fronts.*

Proof. 6.5. Case 1, $\alpha > \beta$: type 1 intersections

Define the tangent vector associated with \mathcal{W}_0^u at the point of intersection as v_0^u and the tangent vector associated with $\mathcal{W}_{u_2}^s$ at the point of intersection as v_0^s . At the point of intersection, v_0^u evolves according to the flow along $\mathcal{W}_{u_2}^s$. Call the resulting vector at the point $(u, s) = (u_2, 0)$ v_f^u and the tangent vector to the stable manifold at that point v_f^s .

Note that, because v_0^u and v_0^s are tangent to the unstable and stable manifolds respectively, their components are determined by the vector field of the corresponding systems, namely (12) and (13). The corresponding matrix is

$$A = \begin{pmatrix} u'_- & u'_+ \\ s'_- & s'_+ \end{pmatrix} \quad (22)$$

and

$$\det(A) = u'_- s'_+ - s'_- u'_+ = (c_1^* - c_2^*) s^2 \quad (23)$$

For intersections of type 1, $c_2^* < \hat{c} < c_1^*$ means $\det(A) > 0$ and the tangent vectors therefore constitute a positively oriented basis for \mathbb{R}^2 . Uniqueness of solutions to differential equations requires that the orientation between the vectors be preserved, so the orientation of the basis associated with $[v_f^u, v_f^s]$ must also be positive.

Next, consider the angular eigenvalue system, obtained by converting the eigenvalue problem associated with (3) to polar coordinates and noting that the equation for θ is independent from that for r , where ω is the streamwise eigenvalue:

$$\dot{\theta} = -(f'(\hat{u}) - \omega) \cos^2 \theta - (c - w(z)) \cos \theta \sin \theta - \sin^2 \theta \quad (24)$$

which has fixed points $\theta_{u/s}^\pm$ corresponding to the unstable/stable directions at $\pm\infty$, given by:

$$\begin{aligned} \theta_{u/s}^+ &= \arctan \left(\frac{-(c + \beta) \pm \sqrt{(c + \beta)^2 + 4(\omega - f'(u_2))}}{2} \right) \\ \theta_{u/s}^- &= \arctan \left(\frac{-(c + \alpha) \pm \sqrt{(c + \alpha)^2 + 4(\omega + l)}}{2} \right) \end{aligned} \quad (25)$$

If a given value of ω is an eigenvalue, the corresponding solution trajectory to (24) with initial condition θ_u^- must approach $\theta_f = \theta_s^+ + n\pi$ as $z \rightarrow \infty$ for some integer n .

Fix $\omega = 0$ and define θ_f as the angle between the positive u axis and v_f^s . A standard argument shows that 0 is not an eigenvalue, so we cannot have $\theta_f = \theta_s^+$. In fact, because of the positive orientation of $[v_f^u, v_f^s]$, it must be that $\theta_f > \theta_s^+$. Because θ_f must be aligned with an invariant subspace at $+\infty$ it must be that $\theta_f = \theta_u^+$ when $\omega = 0$.

Now, because θ_f is a piecewise monotone function of ω , $\omega > 0 \implies \theta_f \geq \theta_u^+$, as varying ω induces counter-clockwise rotation. But, because the vector field along the line $\theta = \frac{\pi}{2}$ is positive, meaning it points in the clockwise direction, θ is unable to rotate through this axis. We conclude that, for $\omega > 0$, $\theta_f = \theta_u^+$ and, by definition, ω is not an eigenvalue. As there are no eigenvalues in the right half plane, type 1 intersections correspond to stable solutions.

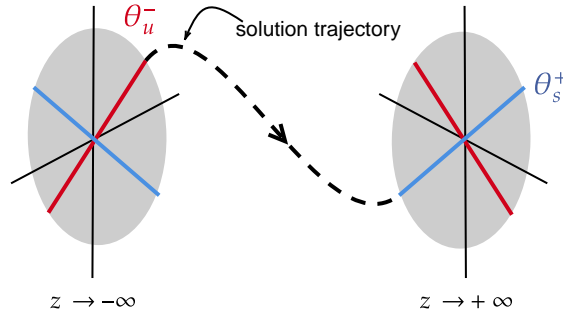


Figure 6: Phase portraits for the angular systems at $-\infty$ and $+\infty$ with a sample solution trajectory moving from θ_u^- to θ_s^+ . Unstable manifolds for each system are indicated in red and stable manifolds in blue.

6.6. Case 2, $\alpha < \beta$: type 2 intersections

In this case, $c_1^* < \hat{c} < c_2^*$ means $\det(A) < 0$ and the basis associated with the tangent vectors $[v_0^u, v_0^s]$ at the point of intersection is negatively oriented, as is the basis associated with $[v_f^u, v_f^s]$.

Again, fix $\omega = 0$. By the same logic as in case 1, 0 is not an eigenvalue: the orientation of $[v_f^u, v_f^s]$ means we must have $\theta_f = \theta_u^+ + \pi$. For $\omega \gg 0$, θ_f approaches θ_u^+ as the growing value of ω overcomes the effect of the nonlinear reaction term. In doing so, it must pass through $\theta_s^+ + \pi$ for some value of $\omega > 0$. Therefore, for intersections of type 2, there is at least one value of ω in the right half plane. The corresponding solution is unstable. \square

The geometric approach described in this section allows us to reconstruct profile solutions and identify the intersection types corresponding to stable profiles. However, we are left with a range of stable—and therefore physically viable—fronts and no means of picking an unique front solution from the continuum of possibilities. In the next two sections, we develop tools to identify the preferred solution.

7. Profile solutions to the boundary value problem with a spatially dependent wind

In §8, we will seek to determine the preferred wave speed and corresponding solution by finding the minimizer of the largest eigenvalue associated with each wave speed/solution pair. This approach requires that we have access to very accurate numerical representations of the solutions whose existence we demonstrated in Proposition 1. As in the constant wind case, we accomplish this by framing our problem as a boundary value problem in which the wave speed c is a free parameter.

The system (5) is defined for $z \in (-\infty, \infty)$, so we look for profile solutions by solving the two-point boundary value problem on this domain, where the problem is given by (5) with wind term (10) and boundary conditions (7). We also have a condition on the derivative of the profile, which takes the form of a pulse:

$$\lim_{z \rightarrow \pm\infty} s = 0 \quad (26)$$

We follow the technique outlined in [19], slightly modified to allow for a discontinuous wind. We employ projective boundary conditions

$$P_{\pm}(U(\pm L) - U_{\pm}) = 0 \quad (27)$$

where $U = (u, s)$, $U_+ = (u_2, 0)$, $U_- = (0, 0)$ and we take $\pm L$ to be sufficiently large so as to approximate numerical infinity.

There exists a one-parameter family of solutions indexed by the wave speed c . To pick a single solution from this family, we specify a phase condition

$$\text{phase}(\gamma) = \gamma u_2 + (1 - \gamma)u_0 \quad (28)$$

for $\gamma \in [0, 1]$. This phase condition serves as an additional boundary condition specifying the spatial location of the center of the profile, which corresponds exactly to the position of the fireline as determined by the point where the derivative $u' = s$ is at a maximum. Imposing a phase condition allows us to leave the wave speed c as an unknown to be solved for, whereas in §7 we specified c and found the intersections of the resulting invariant manifolds in $(u, s(u))$ space.

A number of pre-packaged solvers exist for two-point BVPs, so it is convenient to transform our three-point BVP in to a two-point BVP by doubling the size of the system and halving the domain. Lastly, to account for the unknown wave speed parameter, we augment the system with the additional relation $c' = 0$. Then, (5) becomes

$$\begin{aligned} u'_0 &= s_0 \\ s'_0 &= -(c - w(z))u_0 - f(u_0) \\ u'_1 &= -s_1 \\ s'_1 &= (c - w(z))u_1 + f(u_1) \\ c' &= 0 \end{aligned} \quad (29)$$

for $z \in [0, L]$. To close the system, we introduce a set of matching conditions at the $z = 0$ boundary, resulting in five total boundary conditions for our five-dimensional system. The resulting solutions are smooth profiles asymptotically connecting $u = 0$ to $u = u_2$, as expected.

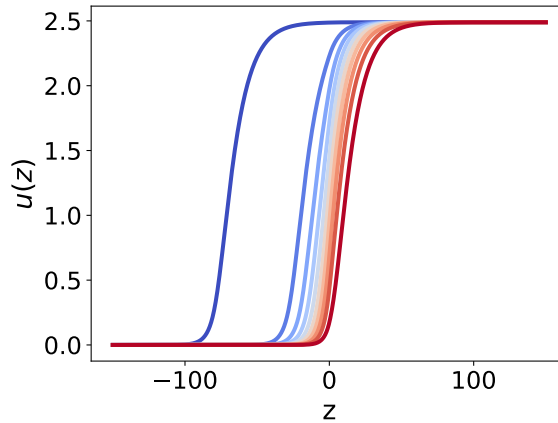


Figure 7: Profile solutions found using the method described in §7, for $v^* = 0.1$, $l = 0.02688$, $\alpha = 0.05$, $\beta = -\alpha$, color-coded by wave speed $c \in [-0.03547, -0.13546]$. In this case, $u_2 \approx 2.5$.

8. Stability as a selection mechanism for the preferred wave

The results presented in Propositions 1 and 2 give us a means of understanding the existence and stability of traveling front solutions to (1) with a spatially dependent wind. In particular, these results affirm our physical intuition: for a divergent wind field—corresponding to $\alpha < \beta$ and type 2 intersections—the front is unstable, whereas for a

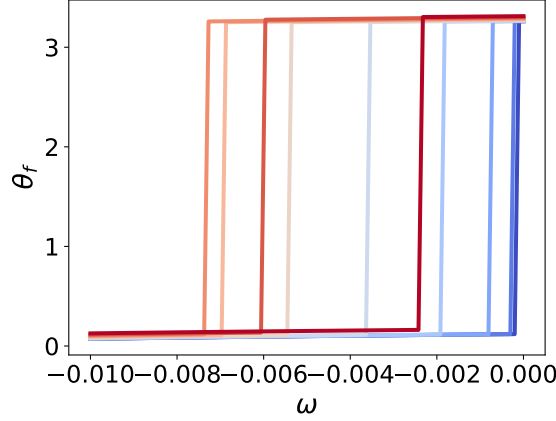


Figure 8: The accumulated angle as a function of ω color-coded by wave speed $c \in [-0.03547, -0.13546]$. Vertical jumps indicate the ω value that is an eigenvalue for that value of c and corresponding solution.

convergent wind—representative of the fire-induced wind described in §1 and corresponding to $\alpha > \beta$ and type 1 intersections—the front is reinforced by the wind field and the solution is stable.

We expect for stable fronts—those whose speeds fall in the range $\hat{c} + \alpha < c < \hat{c} + \beta$ —to persist in nature, so we focus the remainder of our analysis on traveling fronts resulting from type 1 intersections. The solutions we found in §7 for a wind term satisfying this inequality exist for a range of phase conditions, just as intersections of the invariant manifolds discussed in §6 exist for a range of wave speeds. However, without a means of selecting a single wave speed from the continuum of possibilities, the solution for the system with a spatially dependent wind term is not unique.

A reasonable means of identifying the preferred solution is to identify the solution whose largest (meaning least negative) streamwise eigenvalue ω is minimized across possible phase conditions or, equivalently, wave speeds. Because perturbations to this solution will decay the fastest, it is in a sense the “most stable” of the possible solutions. Out of the continuum of possible stable solutions, this spectrally preferred solution corresponds to the traveling front that will persist in nature.

To find the largest eigenvalue for each profile solution found in §7, we again turn to the angular formulation given in (24). Solutions take the form of trajectories that originate on the unstable manifold of the fixed point $(0, 0)$ for the system at $-\infty$ and terminate on the stable manifold of the fixed point $(u_2, 0)$ for the system at $+\infty$, where the two systems are differentiated by the wind term, as in (12) and (13).

If some value of the eigenvalue parameter ω is in fact an eigenvalue, the corresponding trajectory in the angular system $\theta(z)$ will satisfy the following conditions:

$$\begin{aligned} \lim_{z \rightarrow -\infty} \theta &= \theta_u^- \\ \lim_{z \rightarrow +\infty} \theta &= \theta_s^+ \end{aligned} \tag{30}$$

for θ_u^- and θ_s^+ defined as in (25).

To determine if a particular value of ω satisfies this condition, we employ a shooting method, solving (24) by integrating forward in z with initial condition $\theta_0 = \theta_u^-$ and \hat{u} given by the solutions to the BVP discussed in §7.

For each candidate value of ω , we consider $\theta_f(\omega)$, always initializing at $\theta_0 = \theta_u^-$. The final value of the $\theta(z)$ can be thought of as the angle “accumulated” over the course of the trajectory. A jump of size π in the accumulated angle indicates that the corresponding ω value is an eigenvalue, as such a jump can only be achieved if θ_f has moved from θ_u^+ to $\theta_u^+ + \pi$, passing through θ_s^+ or $\theta_s^+ + \pi$ in the process and therefore satisfying condition (30).

The jump we find for each solution for the parameter ranges indicated in figure 7 is never larger than $\Delta\theta = \pi$. An application of Sturm-Liouville theory tells us that, for each solution, this eigenvalue is the first in a string of eigenvalues ordered $\omega_0 > \omega_1 > \dots > -\infty$ and, therefore, the largest.

Finally, we use a root finding algorithm to identify the exact values of ω at which these jumps occur. Examining the largest eigenvalue as a function of the wave speed (alternatively, the phase) for solutions associated with that

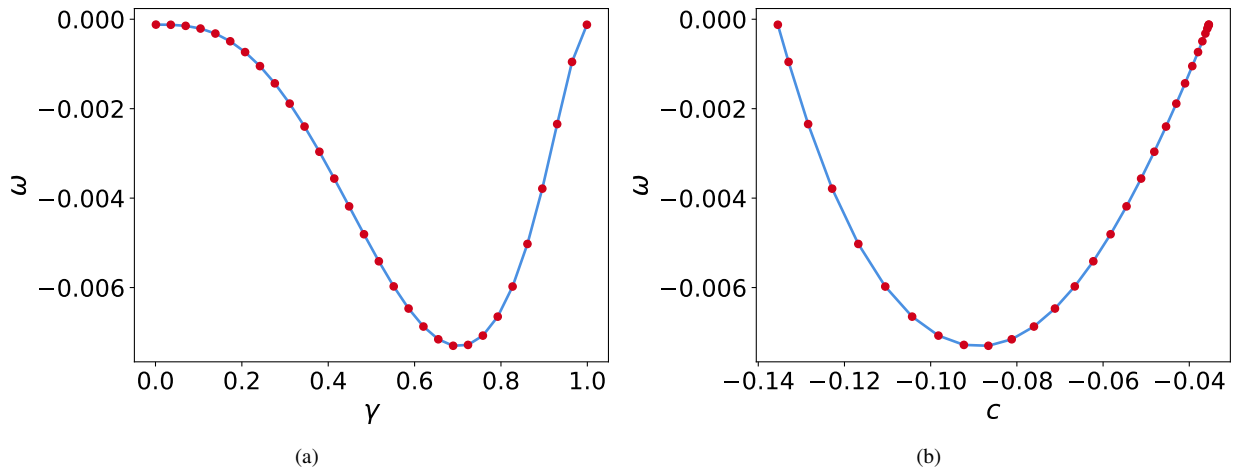


Figure 9: The largest eigenvalue ω as a function of the phase γ in figure (a) and the wave speed c in figure (b). Both views demonstrate a clear minimum and an inverted parabolic structure.

wave speed (phase) gives us a curve with a clear minimum: see figure 9. The solution corresponding to this minimum eigenvalue is the most stable, and therefore preferred, solution.

Note that both eigenvalue curves are essentially inverted parabolas, with ω only approaching 0 as γ and c approach the limits of their respective ranges. This occurs for the limiting cases of $c = \hat{c} + \beta$ and $c = \hat{c} + \alpha$, either end of the range of allowable speeds found in §6. It is only for these limiting cases that an eigenvalue exists at or very near zero: for all other allowable wave speeds, there is no zero eigenvalue and therefore no translational invariance.

For the phase space trajectories corresponding to both limiting situations and the preferred case, as well as the distance between the fireline and wind switch in each case, see figure 10. For wind speeds near the ends of the allowable range, the wind switch occurs very close to $z = \pm\infty$ and far away from the fireline. The preferred solution corresponds to a wave speed of $c = -0.08995$.

Notably, for the preferred solution, the wind switch is closer to the fireline than either of the limiting cases as well as being spatially “ahead.” Specifically, if we compute the signed distance between the u value of the wind switch and that of the fireline as $\mathbf{d} = u_{\text{windswitch}} - u_{\text{fireline}}$, we find $\mathbf{d} = 0.58459$ for the preferred wave speed (as illustrated in image (c) in figure 10). We parameterize the front solutions so that $z = 0$ corresponds to the fireline. Therefore $\mathbf{d} > 0$ means that, for the preferred solution, the wind switch occurs ahead of the fireline in a manner consistent with the physics of air entrainment.

9. Conclusion

Understanding the effects of changes in local environmental variables such as wind on the spatial structure of a propagating fireline is key to better understanding fire behavior more generally. Mathematically, the existence and stability of traveling wave solutions in a system with spatial discontinuities, such as those imposed by the wind switch studied here, is an intriguing extension to classical theory. In this paper, we explored the effects of an external forcing term describing the fire-induced wind on the existence of profiles in the temperature representing fire fronts and their resilience to spatial perturbations.

Traveling wave solutions are heteroclinic connections between fixed points of the corresponding system—in this case, in \mathbb{R}^2 . As such, problems concerning their existence and stability lend themselves well to geometric dynamical systems approaches. We extended the classical existence argument involving the coincidence of invariant manifolds to a spatially discontinuous system, in which existence must be demonstrated through the intersection of invariant manifolds because of the difference between the systems at $\pm\infty$. We found that intersections, and therefore solutions, exist only for a bounded continuum of wave speeds. Moreover, the interval of wave speeds for which solutions exist is dependent on the relative magnitude of the wind speed before and after the point of discontinuity. The relationship

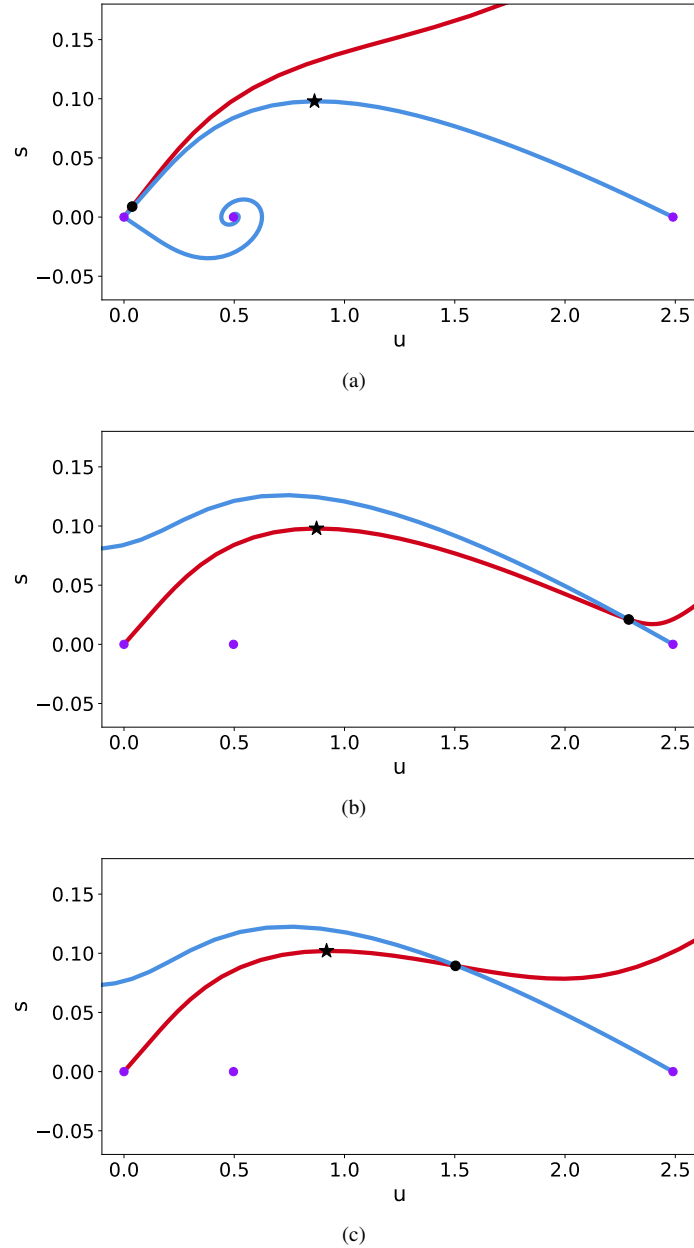


Figure 10: Intersecting invariant manifolds for two wave speeds on either end of the allowed range as well as the preferred wave speed. The fireline occurs at the maximum value of s along the portion of the trajectory corresponding to the solution and is indicated by the black star. The wind switch occurs at the point of intersection of the manifolds and is indicated by the black dot. All intersections are type 1. (a) shows the intersection when c is very close to $\hat{c} + \beta$. The signed distance between the fireline and the wind switch is $\mathbf{d} = -0.82683$. (b) shows the intersection when c is very close to $\hat{c} + \alpha$, with $\mathbf{d} = 1.41559$. (c) shows the intersection for the preferred wave speed, $c = -0.08995$, with $\mathbf{d} = 0.58459$.

between the wind speed parameters also determines which of two qualitatively different categories the intersection falls in to: type 1 or type 2. This classification is tied to the stability of the fronts and allows us to filter out those wind configurations corresponding to unstable—and therefore physically unviable—fronts.

As a means of identifying the spectrally preferred front and its speed, we calculated the magnitude of the largest eigenvalue across the range of wave speeds for which stable fronts exist. This led us to two physical conclusions: firstly, the largest eigenvalue is smaller than zero, as ω only approaches zero very near to the endpoint of the allowed

range of wave speeds and the preferred speed is near the center of the range. The lack of a zero eigenvalue means that translational invariance is broken, so the fronts are localized in space. Secondly, the distance between the fireline and the wind switch is relatively close for the preferred solution, with the wind switch occurring ahead of the fireline.

Ultimately, we are able to use the mathematical criteria for existence and stability of front solutions to determine constraints on the physical configuration of the wind field and its spatial relationship to the fireline. We modeled only the temperature of the fire layer and imposed the combined ambient and fire-induced wind as an external forcing. We found that, for the spectrally preferred solution, the wind switch occurs ahead of the fireline. Despite not explicitly modeling the wind field, this key physical takeaway is consistent with the physics of air entrainment seen in fires at all scales.

CRedit authorship contribution statement

Olivia Chandrasekhar: Writing – original draft, Writing – review & editing, Formal analysis, Conceptualization, Visualization, Funding acquisition. **Christopher Jones:** Writing – review & editing, Formal analysis, Conceptualization, Supervision. **Blake Barker:** Writing – review & editing, Software, Validation. **Rod Linn:** Writing – review & editing, Supervision, Funding acquisition.

Declaration of competing interests

Blake Barker serves on the early career editorial board of *Physica D: Nonlinear Phenomena*. Chris Jones serves on the honorary editorial board of *Physica D: Nonlinear Phenomena*. All other authors declare that they have no known competing financial interests or personal relationships that could have appeared to influence the work reported in this paper.

Acknowledgements

O.C. was supported by the National Science Foundation Graduate Research Fellowship under Grant No. DGE-2439854. O.C. and R.L. were supported by the LDRD Grant “Fighting Fire with Fire: Enabling a Proactive Approach to Wildland Fire” No. 20220024DR. C.J. was supported by Office of Naval Research Grant N00014-24-1-2198.

Supporting materials

The code for profile generation, as described in §7, uses STABLAB [20]. The code for the analysis and figures in this paper is available as part of the STABLAB repository at https://github.com/nonlinear-waves/stablab_matlab/tree/master/streamwise_wildfire and in a stand-alone format at https://github.com/o-chandra/streamwise_wildfire.

References

- [1] J. Mandel, L. S. Bennethum, J. D. Beezley, J. L. Coen, C. C. Douglas, M. Kim, A. Vodacek, A wildland fire model with data assimilation, *Mathematics and Computers in Simulation* 79 (3) (2008) 584–606. doi:<https://doi.org/10.1016/j.matcom.2008.03.015>.
- [2] J. Norbury, A. M. Stuart, Travelling combustion waves in a porous medium. part i—existence, *SIAM Journal on Applied Mathematics* 48 (1) (1988) 155–169. doi:<https://doi.org/10.1137/0148007>.
- [3] J. Norbury, A. M. Stuart, Travelling combustion waves in a porous medium. part ii—stability, *SIAM Journal on Applied Mathematics* 48 (2) (1988) 374–392. doi:<https://doi.org/10.1137/0148019>.
- [4] A. Ghazaryan, S. Lafortune, P. McLarnan, Stability analysis for combustion fronts traveling in hydraulically resistant porous media, *SIAM Journal on Applied Mathematics* 75 (3) (2015) 1225–1244. doi:<https://doi.org/10.1137/140981204>.
- [5] J. Hilton, A. Sullivan, W. Swedosh, J. Sharples, C. Thomas, Incorporating convective feedback in wildfire simulations using pyrogenic potential, *Environmental Modelling & Software* 107 (2018) 12–24. doi:<https://doi.org/10.1016/j.envsoft.2018.05.009>.
- [6] C. Lautenberger, Wildland fire modeling with an Eulerian level set method and automated calibration, *Fire Safety Journal* 62 (2013) 289–298. doi:<https://doi.org/10.1016/j.firesaf.2013.08.014>.
- [7] V. Mallet, D. E. Keyes, F. E. Fendell, Modeling wildland fire propagation with level set methods, *Computers & Mathematics with Applications* 57 (7) (2009) 1089–1101. doi:<https://doi.org/10.1016/j.camwa.2008.10.089>.
- [8] A. L. Atchley, R. Linn, A. Jonko, C. Hoffman, J. D. Hyman, F. Pimont, C. Sieg, R. S. Middleton, Effects of fuel spatial distribution on wildland fire behaviour, *International Journal of Wildland Fire*. 30: 179–189. 30 (2021) 179–189. doi:<https://doi.org/10.1071/WF20096>.
- [9] R. R. Linn, P. Cunningham, Numerical simulations of grass fires using a coupled atmosphere–fire model: Basic fire behavior and dependence on wind speed, *Journal of Geophysical Research: Atmospheres* 110 (D13) (2005). doi:<https://doi.org/10.1029/2004JD005597>.

- [10] J. M. Canfield, R. R. Linn, J. A. Sauer, M. Finney, J. Forthofer, A numerical investigation of the interplay between fireline length, geometry, and rate of spread, *Agricultural and Forest Meteorology* 189-190 (2014) 48–59. doi:<https://doi.org/10.1016/j.agrformet.2014.01.007>.
- [11] R. M. Nelson, B. W. Butler, D. R. Weise, Entrainment regimes and flame characteristics of wildland fires, *International Journal of Wildland Fire* 21 (2) (2012) 127. doi:<https://doi.org/10.1071/WF10034>.
- [12] R. Linn, J. Canfield, P. Cunningham, C. Edminster, J.-L. Dupuy, F. Pimont, Using periodic line fires to gain a new perspective on multi-dimensional aspects of forward fire spread, *Agricultural and Forest Meteorology* 157 (2012) 60–76. doi:<https://doi.org/10.1016/j.agrformet.2012.01.014>.
- [13] S. Dipierro, E. Valdinoci, G. Wheeler, V.-M. Wheeler, A simple but effective bushfire model: Analysis and real-time simulations, *SIAM Journal on Applied Mathematics* 84 (4) (2024) 1504–1514. doi:<https://doi.org/10.1137/24M1644596>.
- [14] B. Sandstede, Stability of travelling waves, in: *Handbook of dynamical systems*, Vol. 2, Elsevier, 2002, pp. 983–1055.
- [15] L. C. Evans, *Partial differential equations*, American Mathematical Society, Providence, R.I., 2010.
- [16] D. Henry, *Geometric Theory of Semilinear Parabolic Equations*, Springer, 1981.
- [17] D. Sattinger, On the stability of waves of nonlinear parabolic systems, *Advances in Mathematics* (1976). doi:[https://doi.org/10.1016/0001-8708\(76\)90098-0](https://doi.org/10.1016/0001-8708(76)90098-0).
- [18] J. M. Paul C. Fife, The approach of solutions of nonlinear diffusion equations to travelling front solutions, *Archive for Rational Mechanics and Analysis* (1977). doi:<https://doi.org/10.1007/BF00250432>.
- [19] L. J. E. e. a. Barker B., Humpherys J., Evans function computation for the stability of travelling waves, *Philos Trans A Math Phys Eng Sci.* (2018). doi:<https://doi.org/10.1098/rspa.1997.0062>.
- [20] B. Barker, J. Humpherys, J. Lytle, K. Zumbun, *Stablab: A matlab-based numerical library for evans function computation* (2015). URL <https://github.com/nonlinear-waves>